THE JOURNAL OF BIOLOGICAL CHEMISTRY VOL. 284, NO. 8, pp. 5010–5020, February 20, 2009

In Situ Mitochondrial Ca^{2+} Buffering Differences of Intact Neurons and Astrocytes from Cortex and Striatum*[S]

Received for publication, September 25, 2008, and in revised form, December 19, 2008 Published, JBC Papers in Press, December 22, 2008, DOI 10.1074/jbc.M807459200

Jorge M. A. Oliveira[1] **and Jorge Gonçalves**

From the REQUIMTE, Serviço de Farmacologia, Faculdade de Farmácia, Universidade do Porto, Rua Aníbal Cunha 164, Porto 4050-047, Portugal

The striatum is particularly vulnerable to neurological disorders, such as Huntington disease. Previous studies, with nonsynaptic mitochondria isolated from cortical and striatal homogenates, suggest that striatal mitochondria are highly vulnerable to Ca^{2+} loads, possibly influencing striatal vulnerability. However, whether and how neuronal and glial mitochondria from cortex and striatum differ in Ca^{2+} vulnerability remains unknown. We test this hypothesis using a novel strategy allowing comparisons of mitochondrial Ca^{2+} buffering capacity in cortical and striatal neuron-astrocyte co-cultures. We provide original evidence that mitochondria not only in neurons but also in astrocytes from striatal origin exhibit a decreased Ca^{2+} buffering capacity when compared with cortical counterparts. The decreased mitochondrial Ca^{2+} buffering capacity in striatal *versus* cortical astrocytes does not stem from variation in mitochondrial concentration or in the rate of intracellular Ca^{2+} elevation, being mechanistically linked to an increased propensity to undergo cyclosporin A (CsA)-sensitive permeability transition. Indeed, 1 μM CsA selectively increased the mitochondrial Ca^{2+} buffering capacity of striatal astrocytes, without modifying that of neurons or cortical astrocytes. Neither thapsigargin nor FK506 modified mitochondrial Ca^{2+} buffering differences between cell types, excluding a predominant contribution of endoplasmic reticulum or calcineurin. These results provide additional insight into the mechanisms of striatal vulnerability, showing that the increased Ca^{2+} vulnerability of striatal *versus* cortical mitochondria resides in both intact neurons and astrocytes, thus positioning the striatum at greater risk for disturbed neuron-astrocyte interactions. Also, the selective effect of CsA over striatal astrocytes suggests that *in vivo* neuronal sheltering with this compound may indirectly result from astrocytic protection.

Brain regions and cell types vary in their susceptibility to neurological disorders. The striatum is particularly vulnerable to both acute (*e.g.* hypoglycemia, hypoxia, and global ischemia) and chronic (*e.g.* Huntington disease (HD)[2]) disorders. Excitotoxicity and altered energy metabolism have been proposed as important determinants of striatal pathogenesis, leading to toxic increases in $[Ca^{2+}]_i$ (1). Studies with mitochondria isolated from brain homogenates raised the hypothesis that striatal mitochondria are more vulnerable to Ca^{2+} loads than cortical mitochondria, possibly contributing to selective striatal vulnerability in pathologies such as HD (2). However, because isolated mitochondria are deprived from its physiological cellular context, and brain homogenates contain mitochondria from both neurons and glia, two fundamental questions remain unanswered: first, whether the differences in Ca^{2+} vulnerability, observed with isolated mitochondria, also occur *in situ* (*i.e.* when mitochondria are in their physiological environment inside intact cells) and, second, whether mitochondrial vulnerability to Ca^{2+} loads differs among neurons and glia from cortex and striatum.

Striatal selectivity in HD is noteworthy, given that the disease-causing protein (mutant huntingtin) is widely expressed throughout the brain and not enriched in the striatum (3). Although HD may also affect nonstriatal regions, namely the cortex (4), typical striatal atrophy and neuronal loss greatly exceed those seen in nonstriatal regions, particularly when HD is not superimposed with Alzheimer's disease or age-related volumetric loss (5). This suggests that vulnerability factors inherent to striatal neurons shape the selective pattern of HD neurodegeneration. One likely factor is the enrichment in *N*-methyl-D-aspartate (NMDA) receptors containing NR2B subunits, allowing prolonged Ca^{2+} influx following excitotoxic stimuli (6), but other vulnerability factors may assist. Mitochondria have an essential role in neuronal survival following excitotoxic $[Ca^{2+}]_i$ elevations (7), and mitochondria-dependent Ca^{2+} handling is impaired in striatal neurons from HD mice (8). HD may in fact be aggravating inherent mitochondrial vulnerability in the striatum, which may reside in either neurons or glia. Indeed, glia may also contribute for non-cell-autonomous neurodegeneration in HD (9) or ischemic injuries (10, 11), thus stressing the importance of identifying vulnerability factors in both neurons and glia.

In the present study, we test the hypothesis that mitochondrial vulnerability to Ca^{2+} loads differs among intact neurons and astrocytes from cortex and striatum. We prepared primary neuron-astrocyte co-cultures from rat cortex and striatum,

* The costs of publication of this article were defrayed in part by the payment of page charges. This article must therefore be hereby marked "*advertisement*" in accordance with 18 U.S.C. Section 1734 solely to indicate this fact.

[S] The on-line version of this article (available at http://www.jbc.org) contains supplemental Figs. 1–3.

[1] To whom correspondence should be addressed. E-mail: jorgemao@ff.up.pt.

[2] The abbreviations used are: HD, Huntington disease; CsA, cyclosporin A; CypD, cyclophilin D; DIV, days *in vitro*; ER, endoplasmic reticulum; FCCP, carbonylcyanide-*p*-(trifluoromethoxyphenyl) hydrazone; FK506, tacrolimus; GFAP, glial fibrillary acidic protein; MK-801, (5*R*,10*S*)-(+)-5-methyl-10,11-dihydro[*a*,*d*]cyclohepten-5,10-imine hydrogen maleate; NMDA, *N*-methyl-D-aspartate; NMDAR, NMDA receptor; PMPI, plasma membrane potential indicator; ROI, region of interest; $TMRM^+$, tetramethylrhodamine methyl ester; ANOVA, analysis of variance.

whose cellular composition and functional differentiation were confirmed by immunolabeling and functional imaging studies, respectively. Here we report for the first time not only the development but also the application of an experimental strategy allowing comparisons of *in situ* mitochondrial Ca^{2+} buffering capacity in the preserved physiological context of intact brain cells. To allow balanced comparisons, similarly to standard procedures with isolated mitochondria experiments, we have introduced calibrations for differences in mitochondrial concentration and rate of intracellular Ca^{2+} elevation in intact cells.

Results in the present study provide additional insight into the mechanisms of striatal vulnerability, showing for the first time that the increased vulnerability of striatal mitochondria to Ca^{2+} loads is present in both intact neurons and astrocytes when compared with their cortical counterparts. Interestingly, our finding of a lower mitochondrial Ca^{2+} buffering capacity in intact striatal *versus* cortical astrocytes, mechanistically linked to increased cyclosporin A-dependent permeability transition, positions the striatum at higher risk for disturbed interactions between two synaptic partners, neurons and astrocytes.

EXPERIMENTAL PROCEDURES

Materials—Fura-4F acetoxymethyl ester, tetramethylrhodamine methyl ester ($TMRM^+$), and 4-bromocalcimycin were from Invitrogen. Plasma membrane potential indicator (PMPI) (Component A from the R-8042 membrane potential assay kit) was from Molecular Devices Corp. (Sunnyvale, CA) (12). Culture media and supplements were from Invitrogen unless otherwise stated. NMDA, (5*R*,10*S*)-(+)-5-methyl-10,11-dihydro[*a*,*d*]cyclohepten-5,10-imine hydrogen maleate (MK-801), ifenprodil, myxothiazol, oligomycin B, rotenone, carbonylcyanide-*p*-(trifluoromethoxyphenyl) hydrazone (FCCP), cyclosporin A, tacrolimus (FK506), thapsigargin, and other reagents were from Sigma.

Cell Culture—Primary cultures were generated from the offspring of Wistar rats (CRIFFA, Barcelona, Spain). Handling and care of animals were conducted according to the European Union guidelines for animal research (86/609/EEC; in agreement with the National Institutes of Health guidelines) and Portuguese law (Portarias 1005/92 and 1131/97). Cortical and striatal cultures were prepared and maintained as previously described for striatal cultures (8, 13) but without cytosine arabinoside to allow the growth of astrocytes. Briefly, hemicortices (free from meninges, olfactory bulb, striatum, and hippocampus) and hemistriata were dissected from the same embryonic day 18 rats, pooled according to brain region (cortex or striatum), and processed in parallel (sister cultures). Dissociated cells (1×10^5) were plated in 12-mm round polyethyleneimine-coated glass coverslips and used in functional imaging experiments between 11 and 13 days *in vitro* (DIV).

Immunocytochemistry—Cells were fixed with 4% paraformaldehyde for 15 min at 37 °C and permeabilized with 0.4% Triton X-100 in phosphate-buffered saline for 15 min. Blocking was performed with 3% bovine serum albumin in phosphate-buffered saline for 30 min at room temperature. Cells were then incubated with primary antibodies for the neuronal marker (mouse anti-MAP-2 (microtubule-associated protein); Sigma; 1:500) and the astrocytic marker (rabbit anti-glial fibrillary acidic protein (GFAP); Dako; 1:250) in 3% bovine serum albumin phosphate-buffered saline for 1 h at room temperature. After washing, cells were incubated with appropriate secondary antibodies conjugated to either AlexaFluor 488 or 594 (Invitrogen; 1:200) for 1 h at room temperature and shielded from light. Nuclei labeling was performed with Hoechst 33342 (Invitrogen; 2 μg/ml; 10 min at room temperature). To test for antibody selectivity, primary antibodies were omitted in control coverslips processed in parallel. No immunolabeling was observed in control coverslips, which were used for shading correction of epifluorescent images, acquired with the same equipment settings.

Monitoring of Dynamic Changes in $[Ca^{2+}]_i$, Mitochondrial Membrane Potential ($\Delta\psi_m$), and Plasma Membrane Potential ($\Delta\psi_p$) in Single Cells—Functional imaging at single-cell resolution was performed with a system composed by an inverted epifluorescence microscope (Eclipse TE300, Nikon, Tokyo, Japan) equipped with 20×, 40×, and 60× air objectives, a monochromator (Polychrome II; TILL Photonics, Martinsried, Germany), a CCD camera (C6790; Hamamatsu Photonics, Hamamatsu, Japan), and a computer with analysis software (Aquacosmos 2.5; Hamamatsu Photonics). Cells were loaded with the $[Ca^{2+}]_i$ probe Fura-4F (5 μM) for 45 min at 37 °C. For simultaneous recordings of changes in $[Ca^{2+}]_i$ and in $TMRM^+$ fluorescence (indicative of changes in $\Delta\psi_m$), 50 nM $TMRM^+$ (quench mode) (14). was present during Fura-4F loading and throughout the experiments. Simultaneous recordings of changes in $[Ca^{2+}]_i$ and in $\Delta\psi_p$ were performed in Fura-4F-loaded cells with a constant PMPI concentration present throughout the experiment. The PMPI concentration was the same as previously described (12), corresponding to a 1:2,000 dilution of a PMPI stock solution prepared by reconstituting one R-8042 Component A vial in 1 ml of ultrapure water. Experiments were performed at 37 °C in buffer containing 133 mM NaCl, 5 mM KCl, 1 mM Na_2SO_4, 0.4 mM KH_2PO_4, 20 mM HEPES, 1.3 mM $CaCl_2$, and 15 mM glucose, pH 7.4. Where indicated, glucose was replaced by 2 mM 2-deoxy-D-glucose, and mitochondria were energized with 10 mM pyruvate. Fura-4F was excited at 340 and 380 nm, $TMRM^+$ at 550 nm, and PMPI at 500 nm. Dual Fura-4F and $TMRM^+$ emission was collected with a 73100bs dichroic and a 73101m emitter (Chroma Technology Corp., Rockingham, VT), whereas dual Fura-4F and PMPI emission was collected with a 505-nm beam splitter and a 520-nm long pass filter. There was no significant bleed-through between Fura-4F and $TMRM^+$ or between Fura-4F and PMPI with these excitation and emission settings. Individual cells were identified as regions of interest (ROIs) for the determination of fluorescence time courses.

In situ calibration of Ca^{2+} responses for each individual cell was performed at the end of every experiment, according to previously detailed procedures (8). Briefly, maximal 340/380 ratios (R_{max}) were determined with 20 μM 4-bromocalcimycin with 1.3 mM extracellular Ca^{2+}, and minimal 340/380 ratios (R_{min}) were determined in Ca^{2+}-free buffer with 5 mM EGTA. This Ca^{2+}-free buffer contained neither $TMRM^+$ nor PMPI, and thus the subsequent decays in their respective fluorescence should not be interpreted as changes in $\Delta\psi_m$ or $\Delta\psi_p$. In experiments addressing mitochondrial Ca^{2+} buffering capacity, maximal mitochondrial depolarization ($\Delta\psi_m$ collapse) was con-

firmed/evoked before $[Ca^{2+}]_i$ calibration by adding protonophore (1 μM FCCP), with ATP synthase reversal prevented by oligomycin (3 μM). Further details on the analysis of cellular responses are provided below.

Image Processing and Data Analysis—Analysis of $[Ca^{2+}]_i$ responses was performed as previously detailed (8). Briefly, background-corrected 340/380 Fura-4F ratios were normalized to the R_{max} (100 units) and R_{min} (0 units) determined for each single cell during *in situ* calibration. The *left yy* axes of Ca^{2+} graphs are scaled with these normalized values, where 50 units should correspond to the Ca^{2+} probe K_d, regardless of its absolute value inside the different cells. The *right yy* axis is an approximate log $[Ca^{2+}]_i$ scale adjusted based on the dynamic range of Fura-4F and K_d determinations (15, 16).

Changes in $TMRM^+$ and PMPI fluorescence in single cells are expressed as arbitrary fluorescence units. Individual signals are corrected for epifluorescence shading, using images acquired in the same experimental *xx-yy-zz* plane, without $TMRM^+$ (during R_{min} determination at the end of the experiment) and in the absence of PMPI (before starting the experiment, in PMPI-free buffer). Exposure times for image acquisition were kept constant in all experiments, with signal saturation and underexposure being avoided merely by adjusting camera gain before starting the experiments. Mathematical correction for different gains was introduced so that all fluorescent signals are compared under the same circumstances.

Conversions to mV of neuronal PMPI fluorescence (Figs. 1, *B* and *D* (*ii*), and 2, *A* (*ii*)) were performed in a manner similar to that described previously (12) but with *in situ* calibration for each individual neuron. Briefly, extracellular Na^+ was replaced equimolarly by K^+ in a stepwise fashion, up to 42 mM extracellular K^+ in the assay buffer. $\Delta\psi_p$ values (in mV) were derived from the Goldman-Hodgkin-Katz equation, assuming conductances for K^+, Na^+, and Cl^- of 100:1:100. PMPI fluorescence enhancements evoked by K^+ in each neuron were plotted in a function of $\Delta\psi_p$ and fit monoexponentially (correlation coefficients, $r^2 > 0.990$) to generate individual calibration curves to derive approximate $\Delta\psi_p$ changes in mV.

Cell size was determined from the ROI area (μm^2) using micrometer-calibrated images. Neuronal areas reflect only the soma, due to impossibility of tracing the entire neuronal processes. Area conversion into approximate somatic diameter (*e.g.* Fig. 2*B*) was performed by a circular approximation using Equation 1,

$$d = 2 \times SQRT(a/\pi) \quad \text{(Eq. 1)}$$

where d represents the diameter, *SQRT* is the square root, a is the area, and π is the circular constant.

Mitochondrial concentration in single cells was estimated from the analysis of the average $TMRM^+$ fluorescence in each ROI (for a representative measurement, see Fig. 3*A* (*ii*), *solid line*, $\gamma - \delta$). The difference between resting $TMRM^+$ fluorescence (start of experiment) and nonmitochondrial fluorescence ($TMRM^+$ signal after FCCP, prior to R_{max} determination; Figs. 3 and 4 (*ii*), *solid lines*) was assumed to reflect mitochondrial concentration. Our assumption is based on evidence that when the amount of $TMRM^+$ stacked in the mitochondria surpasses the quench threshold, autoquenching occurs and fluorescence becomes invariant with matrix $TMRM^+$ concentration (14); $TMRM^+$ quenching in the present study is evidenced by the dequenching spikes in Fig. 4, *A–D*, *ii*, *solid lines*). Therefore, the resting cellular $TMRM^+$ fluorescence in our experiments is primarily governed by the amount of mitochondria per cell volume (mitochondrial concentration) with superimposed nonmitochondrial fluorescence. This nonmitochondrial fluorescence reflects $TMRM^+$ in extracellular buffer in the cytosol and nonspecifically bound to cellular elements. Hence, subtracting the residual $TMRM^+$ signal following full $\Delta\psi_m$ collapse (as confirmed with FCCP in the presence of oligomycin) should eliminate the vast majority of nonmitochondrial fluorescence, thus yielding an estimate of mitochondrial concentration. We further substantiate this procedure by providing both medium and high magnification images (supplemental material) of $TMRM^+$-loaded neurons and astrocytes used in functional experiments. Collectively, the images show that the mitochondrial distribution is sparser in astrocytes that in neurons, visually showing a lower mitochondrial concentration. We also provide fluorescence intensity profiles across representative cells as well as time lapse experiments illustrating how $\Delta\psi_m$ collapse with oligomycin plus FCCP influences $TMRM^+$ distribution and fluorescence intensity values in mitochondria-rich and mitochondria-free cellular regions.

The rate of $[Ca^{2+}]_i$ elevation was estimated by curve-fitting (with nonlinear regression) the normalized Fura-4F 340/380 ratios in experiments such as in Fig. 4, where the combination of oligomycin and a respiratory chain inhibitor (myxothiazol) collapsed $\Delta\psi_m$, preventing mitochondrial Ca^{2+} uptake (17). Best fit values, with $r^2 > 0.990$, were obtained with Equation 2,

$$y = IF(\chi < x_0), \text{THEN } y = b, \text{ELSE } y = b + (t - b) \times (1 - e^{(-K_{exp} \times (x - x_0))}) \quad \text{(Eq. 2)}$$

where y represents normalized $[Ca^{2+}]_i$ at time x, x_0 is the first time point, b is basal $[Ca^{2+}]_i$, t is the top part of the curve (constrained to be below the 100 value achieved during R_{max}), e is Neper's number, and K_{exp} is the exponential constant used to compare the rate of $[Ca^{2+}]_i$ elevation among cells (*e.g.* Fig. 4*A* (*i*), K_{exp} *arrow*). It should be noted that myxothiazol, albeit at higher concentrations, was previously shown to inhibit Ca^{2+} influx through store-operated channels (18). However, 3 μM oligomycin (specifically oligomycin B, which has a 0.5 μM K_{50} for the inhibition of store-operated Ca^{2+} influx (19)) was present in our experiments either with or without myxothiazol, thus preventing differences in store-operated Ca^{2+} influx between these experiments.

Image processing was performed with Aquacosmos 2.5 (Hamamatsu Photonics) and with ImageJ (National Institutes of Health; available on the World Wide Web). Calculations on numerical data derived from ROIs were automated in Excel spreadsheets (Microsoft Corp., Redmond, WA). Values throughout are presented as mean ± S.E. unless otherwise stated. Nonlinear regressions, curve fitting, and *t* tests were performed using GraphPad Prism version 4.0 (San Diego, CA). Other statistical analyses were performed with Statistical Package for the Social Sciences version 15.0 for Windows (SPSS Inc., Chicago, IL). Type I error probability was set at 0.05 for all analyses.

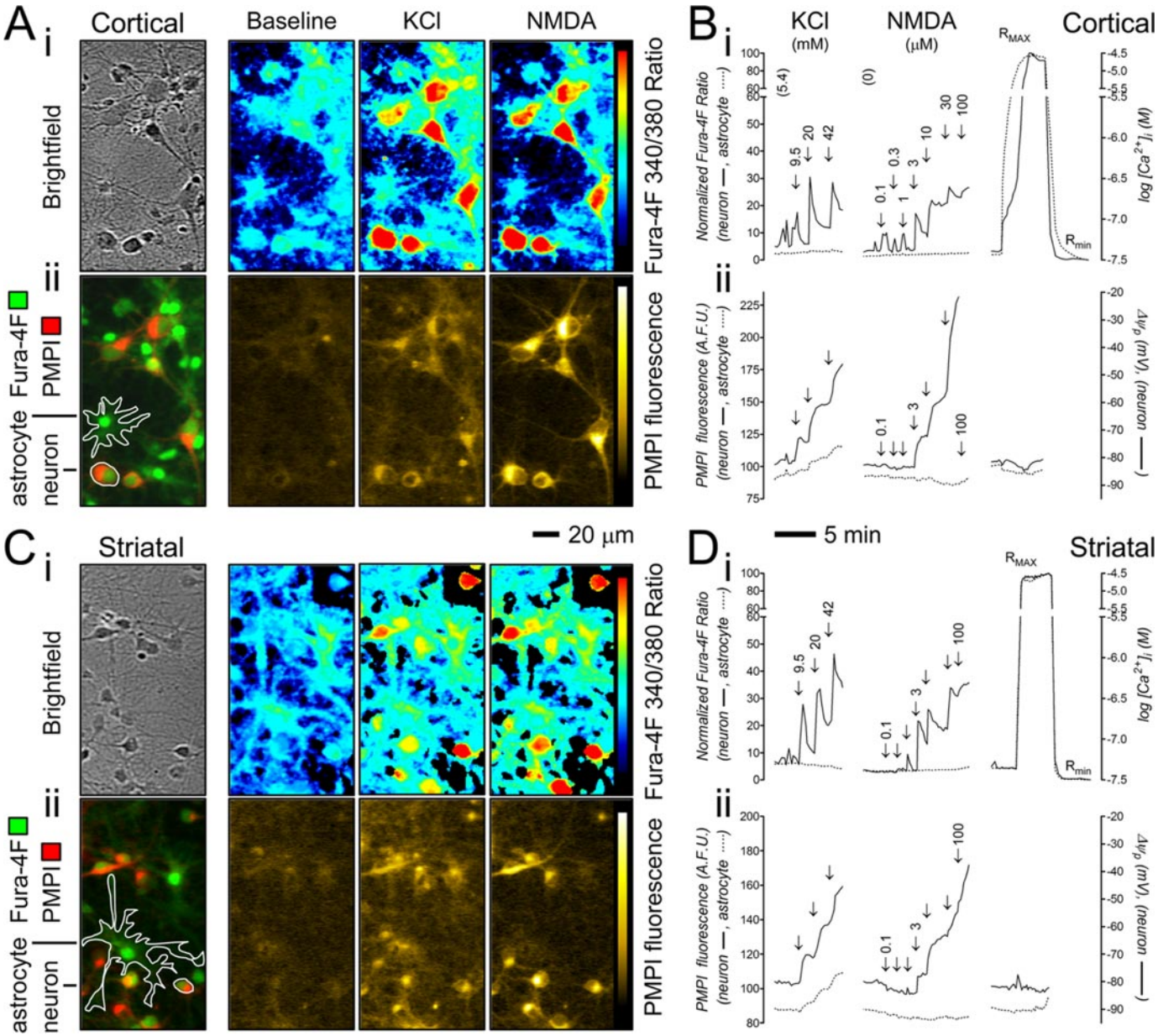

FIGURE 1. **Neurons and astrocytes are functionally differentiated in both cortical and striatal cultures.** *A* and *C*, field excerpts from 20× photos of 11 DIV cortical and striatal cultures, respectively, used in functional imaging experiments with simultaneous recordings of changes in $[Ca^{2+}]_i$ with Fura-4F and $\Delta\psi_p$ with PMPI. *Scale bar*, 20 μm. *B* and *D*, functional $[Ca^{2+}]_i$ (*i*) and $\Delta\psi_p$ (*ii*) responses of single representative neurons (*solid lines*) and astrocytes (*dashed lines*) exposed to the indicated concentrations of KCl and NMDA/glycine (10:1). Data are from a representative experiment with sister cortical and striatal cultures. *Time bar*, 5 min.

RESULTS

Characterization of Neurons and Astrocytes in Cortical and Striatal Cultures—Immunolabeling revealed that cortical and striatal cultures were predominantly composed of neurons and astrocytes (over 95% of all nuclei stained with Hoechst 33342 were also positive for either the neuronal marker, MAP-2, or the astrocytic marker, GFAP) (supplemental Fig. 1). At 11 DIV, cells were functionally differentiated. Neurons responded to K^+ or NMDA receptor (NMDAR) activation with $[Ca^{2+}]_i$ elevation and plasma membrane depolarization in a concentration-dependent manner (Fig. 1, *A* and *C*, and *solid lines* in *B* and *D*). In contrast, astrocytes did not respond to NMDA (up to 100 μM), despite exhibiting changes in plasma membrane polarization upon K^+ challenging. Also, no changes in astrocytic $[Ca^{2+}]_i$ were detected during either K^+ or NMDA challenging, despite clear responses to Ca^{2+}-ionophore during $[Ca^{2+}]_i$ calibration (R_{max}; Fig. 1, *A* and *C*, and *dashed lines* in *B* and *D*). These clear functional differences ensured cellular identification, particularly in experiments with PMPI (*e.g.* Fig. 1, *A* and *C* (*ii*), *bottom left*; Fig. 3, *A* and *B* (*ii*), *dashed lines*).

To appraise differences between cortical and striatal neurons, we integrated three parameters (somatic diameter, NMDA pEC_{50}, and proportion of functional NMDAR-2B) in a cluster analysis with $n = 23$ random neurons of each type. The average somatic diameter was larger for cortical neurons (17.4 ± 0.4 *versus* 12.9 ± 0.2 μm; $p < 0.001$). Despite similar

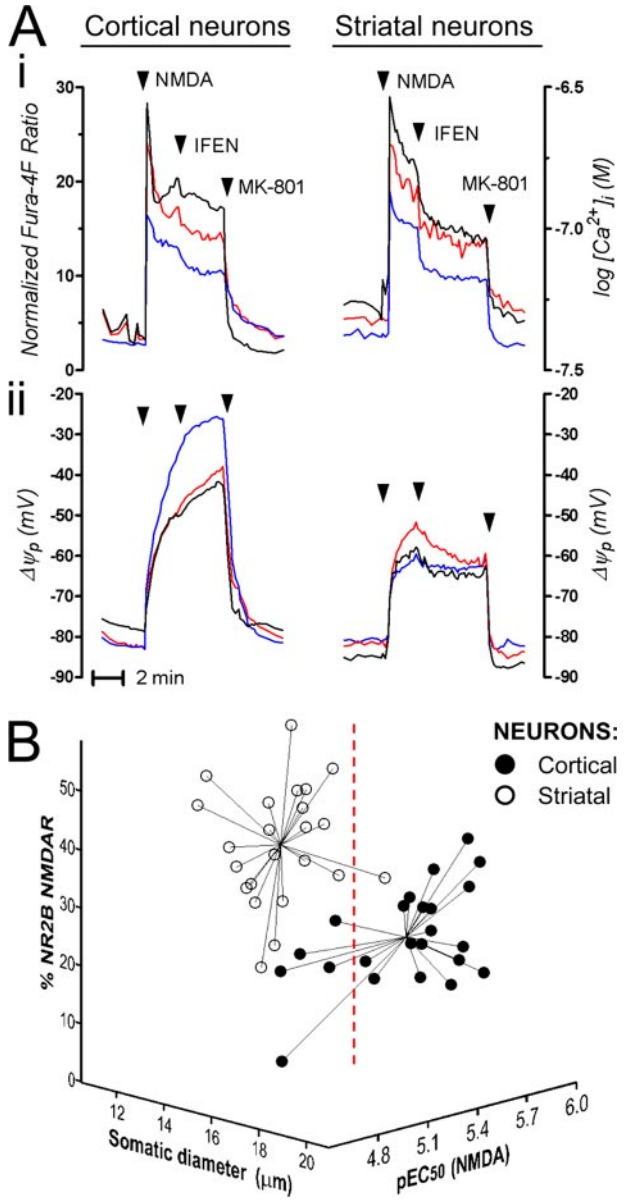

FIGURE 2. **Cultured cortical and striatal neurons are morphologically and functionally distinct.** *A*, simultaneous monitoring of changes in $[Ca^{2+}]_i$ (*i*) and $\Delta\psi_p$ (*ii*) in cortical and striatal neurons. NMDA (10 μM + 1 μM glycine), ifenprodil (*IFEN*; 2 μM), and MK-801 (5 μM) were added where indicated. *Matched color lines* in *i* and *ii* represent measurements performed in the same representative neuron (three are shown for each type). *Time bar*, 2 min. *B*, three-dimensional morphofunctional clustering of cortical (*black circles*) and striatal (*white circles*) neurons using the three parameters in *xx*, *yy*, and *zz*. Data are from a total of 46 (23 cortical and 23 striatal) neurons from single representative experiments with sister cultures. The *solid lines* converge to the respective centroid, and the *vertical red dashed line* divides neurons according to the blinded "two-step cluster analysis."

NMDA pEC_{50} (5.48 ± 0.05 *versus* 5.36 ± 0.05, cortical and striatal neurons, respectively; $p = 0.087$), the contribution of the NMDAR-2B subtype for $[Ca^{2+}]_i$ responses was higher in striatal (37.0 ± 2.1%) *versus* cortical neurons (24.9 ± 1.9%; $p < 0.001$). This latter parameter was derived from the degree of attenuation with ifenprodil (2 μM; selective NMDAR-2B antagonist; IFEN in Fig. 2*A*) of plateau responses to 10 μM NMDA (a concentration close to the NMDA EC_{50}) and is expressed as a percentage of maximal attenuation with MK-801 (5 μM; non-subtype-selective NMDAR antagonist). These three parameters were plotted three-dimensionally, and a "two-step cluster analysis" (Statistical Package for the Social Sciences version 15.0; blind to both the cortical or striatal origin of the data points as well as the expected number of clusters) separated them into two clusters (Fig. 2*B*, *red dashed line*), nearly completely (40:46) matching their brain origin and thus showing strong differences among the two neuronal populations. Meaningfully, these differences are reminiscent of the *in vivo* condition, namely the smaller somatic size of striatal neurons and particularly their higher proportion of functional NMDAR-2B, which is considered a relevant determinant for their selective vulnerability (6, 20).

Interestingly, three-dimensional cluster analysis with morphofunctional parameters also separated neurons and astrocytes with minor overlap (supplemental Fig. 2), showing the potential application of this strategy to automated image analysis. Most importantly, evidence of morphological and functional differences among cells underlines the significance of comparing their mitochondrial properties *in situ*.

In Situ Mitochondrial Ca^{2+} Buffering Capacity in Intact Neurons and Astrocytes—To monitor mitochondrial Ca^{2+} buffering *in situ*, cells were loaded with Fura-4F ($K_d \sim 1$ μM), a probe we have previously shown adequate to identify the mitochondrial set point for Ca^{2+} accumulation (8). Because we aimed as studying intact cells, we avoided standard strategies such as ionophores or proteolytic enzymes as a means to expose mitochondria to Ca^{2+}. Instead, we devised a strategy using a controlled ATP depletion to elevate $[Ca^{2+}]_i$, which was buffered at the expense of $\Delta\psi_m$ by mitochondria energized with the cell-permeable substrate pyruvate (10 mM).

To initiate the Ca^{2+} challenging of *in situ* mitochondria, glycolytic and mitochondrial ATP generation were prevented by replacing glucose with 2-deoxy-D-glucose (2 mM) and by adding the ATP synthase inhibitor oligomycin (3 μM). This procedure initiated an elevation of $[Ca^{2+}]_i$ in both neurons and astrocytes (Fig. 3, *A–D*, *i*, *O*), reaching a "plateau" (Fig. 3*A* (*i*), α point), after which $[Ca^{2+}]_i$ was buffered for a variable period until the onset of a massive increase in $[Ca^{2+}]_i$ (Fig. 3*A* (*i*), β point), suggesting widespread Ca^{2+} overload in the *in situ* mitochondrial population of each single cell, which invariably led to cell death.

Evidence that the above described $[Ca^{2+}]_i$ plateau results from mitochondrial Ca^{2+} buffering is as follows: (i) the plateau occurs at $[Ca^{2+}]_i$ close to the mitochondrial set point for Ca^{2+} accumulation (0.3–1 μM) (7) (Fig. 3, *A–D* (*i*)); (ii) no plateau is observed if mitochondria are prevented from uptaking Ca^{2+} (Fig. 4, *A–D* (*i*)); (iii) the plateau is immediately disrupted, and mitochondrial Ca^{2+} is released to the cytosol, upon $\Delta\psi_m$ collapse with protonophore (1 μM FCCP) (supplemental Fig. 3*B*); (iv) mitochondrial depolarization, as judged from the analysis of $TMRM^+$ redistribution (Fig. 3, *A–D* (*ii*), *solid lines*), is ongoing throughout the $[Ca^{2+}]_i$ plateau and near completion at the time where the plateau can no longer be sustained (Fig. 3, β point).

Measurements of *in situ* mitochondrial Ca^{2+} buffering were thus derived from the time difference between the aforementioned α and β points ($\beta - \alpha$ = duration of the $[Ca^{2+}]_i$ plateau), a procedure that follows the same reasoning applied to isolated

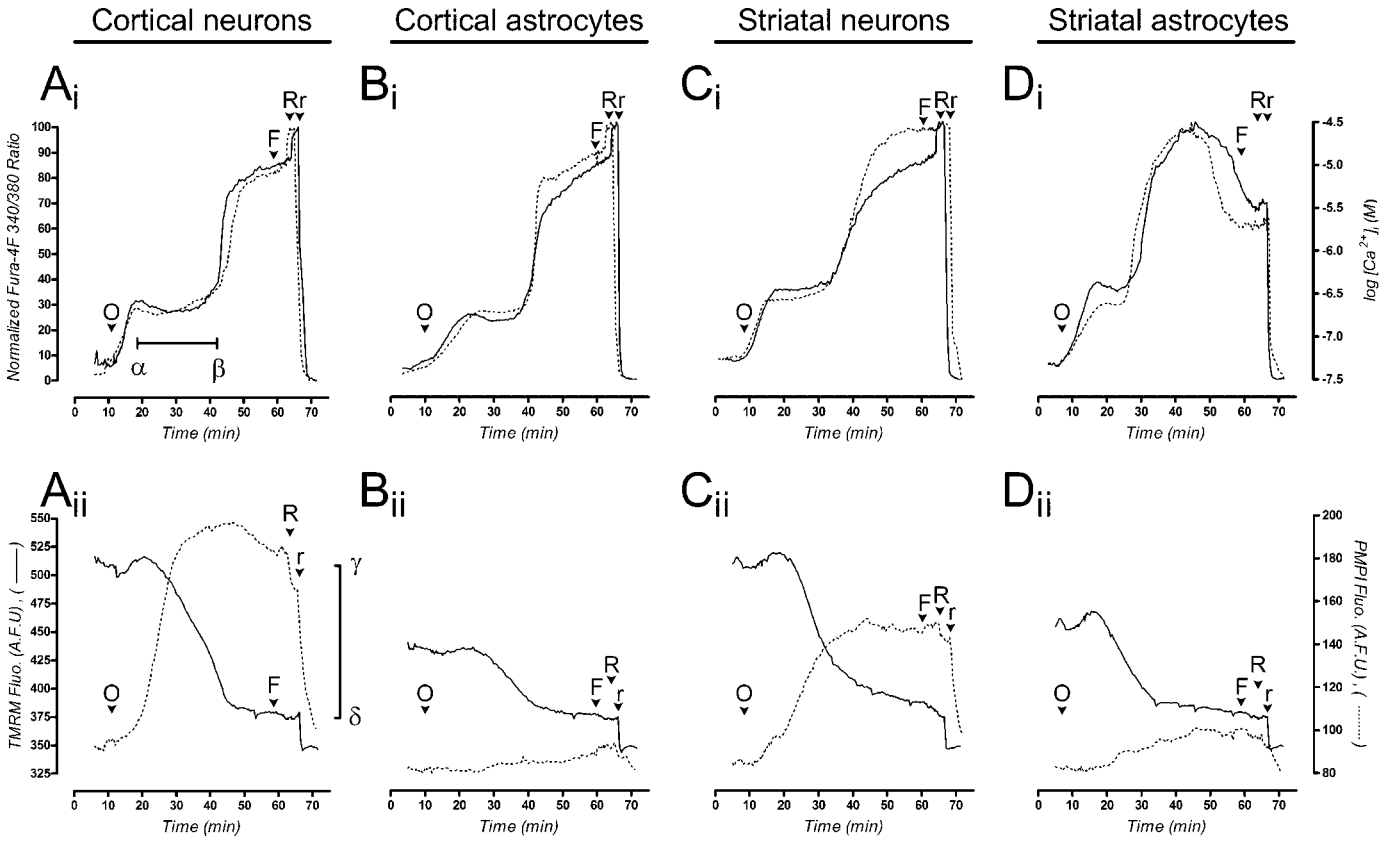

FIGURE 3. ***In situ* monitoring of mitochondrial Ca^{2+} buffering capacity in neurons and astrocytes from cortex and striatum.** *A–D*, changes in $[Ca^{2+}]_i$ (*i*) and in $TMRM^+$ (*ii*; *solid lines*) or PMPI (*ii*; *dashed lines*) fluorescence in arbitrary units (*A.F.U.*). The *solid* or *dashed line* in *i* and *ii* depicts measurements performed simultaneously in the same single cell. Representative cells with identical $[Ca^{2+}]_i$ kinetics were chosen (*i*) in order to allow comparison of changes in $TMRM^+$ and PMPI fluorescence (*ii*). Assay buffer contained 10 mM pyruvate, and glucose was replaced by 2 mM 2-deoxy-D-glucose before the addition of oligomycin (3 μM; *O*). FCCP addition (1 μM; *F*) confirms full $\Delta\psi_m$ collapse. *R* and *r*, R_{max} and R_{min} determinations, respectively. *A* (*i*), $\beta - \alpha$, duration of the $[Ca^{2+}]_i$ plateau (*i.e.* apparent mitochondrial Ca^{2+} buffering). *A* (*ii*), $\gamma - \delta$, mitochondrial concentration. Up to 50 random single cells of each type were analyzed per experiment; only a few are shown for clarity, being representative of $n = 7$ independent experiments.

mitochondria experiments with steady Ca^{2+} infusion (13, 21). Results for the duration of the $[Ca^{2+}]_i$ plateau are shown in Fig. 5*A*, where a two-factor (region × cell type) ANOVA revealed a significant region × cell type interaction ($F_{(1,24)} = 4.63$; $p = 0.042$), a significant main effect of the cell type (neurons *versus* astrocytes; $F_{(1,24)} = 23.7$; $p < 0.001$), and no significant effect of the brain region (cortical *versus* striatal; $F_{(1,24)} = 1.23$; $p = 0.279$).

These results, *per se*, suggest that *in situ* mitochondrial Ca^{2+} buffering capacity is higher in neurons than in astrocytes, with no differences between cortical and striatal neurons, and with mitochondria in striatal astrocytes exhibiting the lowest Ca^{2+} buffering capacity, thus affording the lowest protection and precipitating loss of Ca^{2+} homeostasis and cell death. Still, following a similar reasoning to standard isolated mitochondria experiments, we investigated whether differences in mitochondrial concentrations and/or rate of Ca^{2+} elevation among cell types might be influencing these results.

Mitochondrial Concentration and Rate of $[Ca^{2+}]_i$ Elevation in Intact Neurons and Astrocytes—Because the cellular mitochondrial concentration, and the rate of $[Ca^{2+}]_i$ elevation may affect the time during which intact cells can buffer $[Ca^{2+}]_i$ (more mitochondria or less Ca^{2+} = more time; less mitochondria or more Ca^{2+} = less time), we have assessed whether such parameters differ among neurons and astrocytes from cortical and striatal origin. Mitochondrial concentrations were measured as detailed under "Experimental Procedures" (*e.g.* $\gamma - \delta$ in Fig. 3*A* (*ii*), *solid line*; see also supplemental material). Analysis of $TMRM^+$ fluorescence under matrix quenching conditions (50 nM; as demonstrated by the dequenching spikes in Fig. 4, *A–D* (*ii*), *solid lines*) revealed a higher mitochondrial concentration in neurons than in astrocytes, expressed by a larger difference between the $TMRM^+$ fluorescence before oligomycin and that remaining after FCCP, which reflects nonmitochondrial fluorescence (Figs. 3 and 4, *A* and *C* (*ii*) *versus B* and *D* (*ii*), *solid lines*). Two-factor (region × cell type) ANOVA of the mitochondrial concentration (Fig. 5*B*) revealed a significant main effect of the cell type (neurons *versus* astrocytes; $F_{(1,16)} = 24.5$; $p < 0.001$) and no significant effect of brain region (cortical *versus* striatal; $F_{(1,16)} = 1.11$; $p = 0.308$) nor of region × cell type interaction ($F_{(1,16)} = 0.253$; $p = 0.622$). Hence, these results suggest that the lower "apparent" mitochondrial Ca^{2+} buffering capacity for astrocytes (Fig. 5*A*) is partly due to their lower mitochondrial concentration, when compared with neurons (Fig. 5*B*). Interestingly, despite the differences in the average area of cortical and striatal neuronal somas (~1.2×; 220 ± 4 *versus* 177 ± 4 μm^2, $n = 526$ and 477 neurons, respectively) and especially between cortical and striatal astrocytes (~2.5×; 324 ± 8 *versus* 796 ± 30 μm^2, $n = 472$ and 267 astrocytes, respectively), the mitochondrial concentrations in both types of

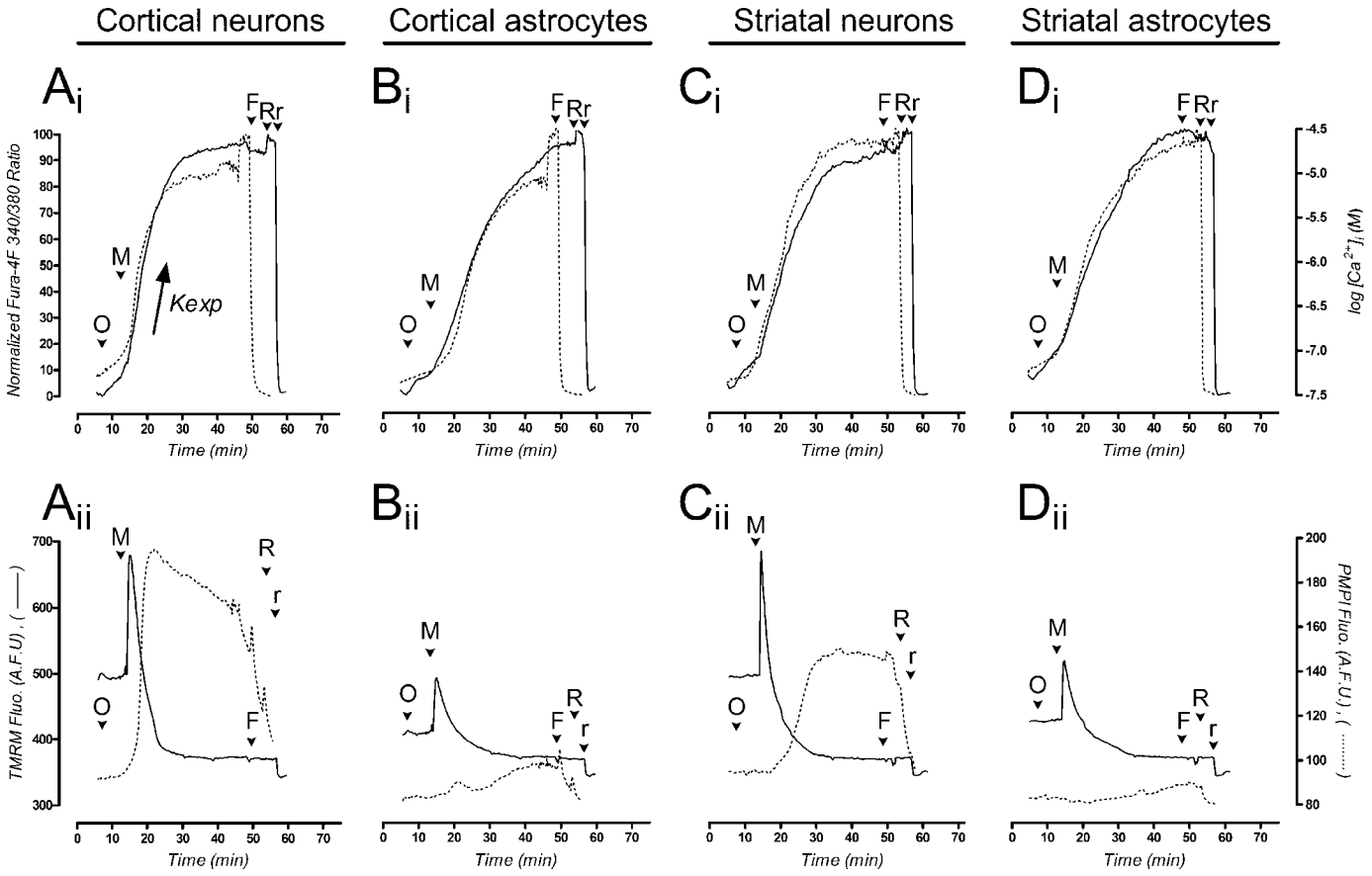

FIGURE 4. **Intracellular Ca^{2+} dynamics in neurons and astrocytes from cortex and striatum under conditions where mitochondria are prevented from buffering $[Ca^{2+}]_i$.** *A–D*, changes in $[Ca^{2+}]_i$ (*i*) and in $TMRM^+$ or PMPI (*ii*; *solid* or *dashed lines*, respectively) fluorescence in arbitrary units (*A.F.U.*). The *solid* or *dashed line* in *i* and *ii* depicts measurements performed simultaneously in the same single cell. *i*, representative cells with identical $[Ca^{2+}]_i$ kinetics to allow comparisons in *ii*. Oligomycin (*O*; 3 μM) and myxothiazol (*M*; 2 μM) were added where indicated. FCCP (*F*; 1 μM) addition and *in situ* determination of R_{max} and R_{min} (*R* and *r*, respectively) were performed at the indicated times for cells depicted by *solid lines* and slightly earlier for those shown by *dashed lines* (*A* and *B*, 10 min earlier; *C* and *D*, 5 min earlier). This time variation results from the need to anticipate and avoid excessive Fura-4F leakage to allow accurate $[Ca^{2+}]_i$ calibration. Assay buffer contained 10 mM pyruvate, and glucose was replaced by 2 mM 2-deoxy-D-glucose before the addition of oligomycin (3 μM). *A* (*i*), K_{exp}, the rate of $[Ca^{2+}]_i$ elevation. Up to 50 random single cells of each type were analyzed per experiment; only a few are shown for clarity, being representative of $n = 5$ independent experiments.

neurons as well as in both types of astrocytes is remarkably similar (Fig. 5*B*). These results show that mitochondrial concentration is primarily governed by the cell type (neurons *versus* astrocytes) rather than by its region of origin (cortical *versus* striatal).

To test whether *in situ* mitochondria of the different cell types were being exposed to different rates of $[Ca^{2+}]_i$ elevation, we performed experiments similar to those depicted in Fig. 3 but with the further addition of myxothiazol (2 μM) after oligomycin (Fig. 4). The underlying reasoning was that although oligomycin allows mitochondrial Ca^{2+} uptake, the combination of oligomycin and a respiratory chain inhibitor (myxothiazol) prevents it by collapsing $\Delta\psi_m$ (17), thus allowing a measurement of the rate at which $[Ca^{2+}]_i$ is rising inside cells, in close analogy with removing mitochondria from the "test tube" and measuring the rate at which Ca^{2+} is being infused in isolated mitochondria experiments (13). Indeed, with myxothiazol present, $\Delta\psi_m$ in both neurons and astrocytes rapidly collapsed (Fig. 4, *A–D* (*ii*), *solid lines*; $TMRM^+$ dequenching), and the $[Ca^{2+}]_i$ elevation initiated with oligomycin progressed without interruption until near Fura-4F saturation, showing the absence of mitochondrial Ca^{2+} uptake (Fig. 4, *A–D* (*i*); compare with Fig. 3, *A–D* (*i*)). By means of nonlinear regression with Equation 2, as detailed under "Experimental Procedures," we calculated the rate constant, K_{exp}, allowing comparisons of the rate of $[Ca^{2+}]_i$ elevation among cell types. Two-factor (region × cell type) ANOVA of this parameter (Fig. 5*C*) revealed a significant region × cell type interaction ($F_{(1,16)} = 14.5$; $p = 0.002$) as well as a significant main effect of the cell type (neurons *versus* astrocytes; $F_{(1,16)} = 8.45$; $p = 0.010$) and of the brain region (cortical *versus* striatal; $F_{(1,16)} = 11.2$; $p = 0.004$). These results show that mitochondria in cortical neurons are exposed to a significantly higher rate of $[Ca^{2+}]_i$ elevation when compared with the other cell types (cortical astrocytes, striatal neurons, or striatal astrocytes) for which similar rates were observed. Hence, the absence of differences in mitochondrial Ca^{2+} buffering between cortical and striatal neurons depicted in Fig. 5*A* is only "apparent." Indeed, in order to buffer for similar periods a faster rate of Ca^{2+} elevation with identical mitochondrial concentrations, cortical neurons should possess mitochondria with higher Ca^{2+} buffering capacities than striatal neurons.

To allow comparisons of the present *in situ* mitochondrial Ca^{2+} buffering data with what should be expected if the mito-

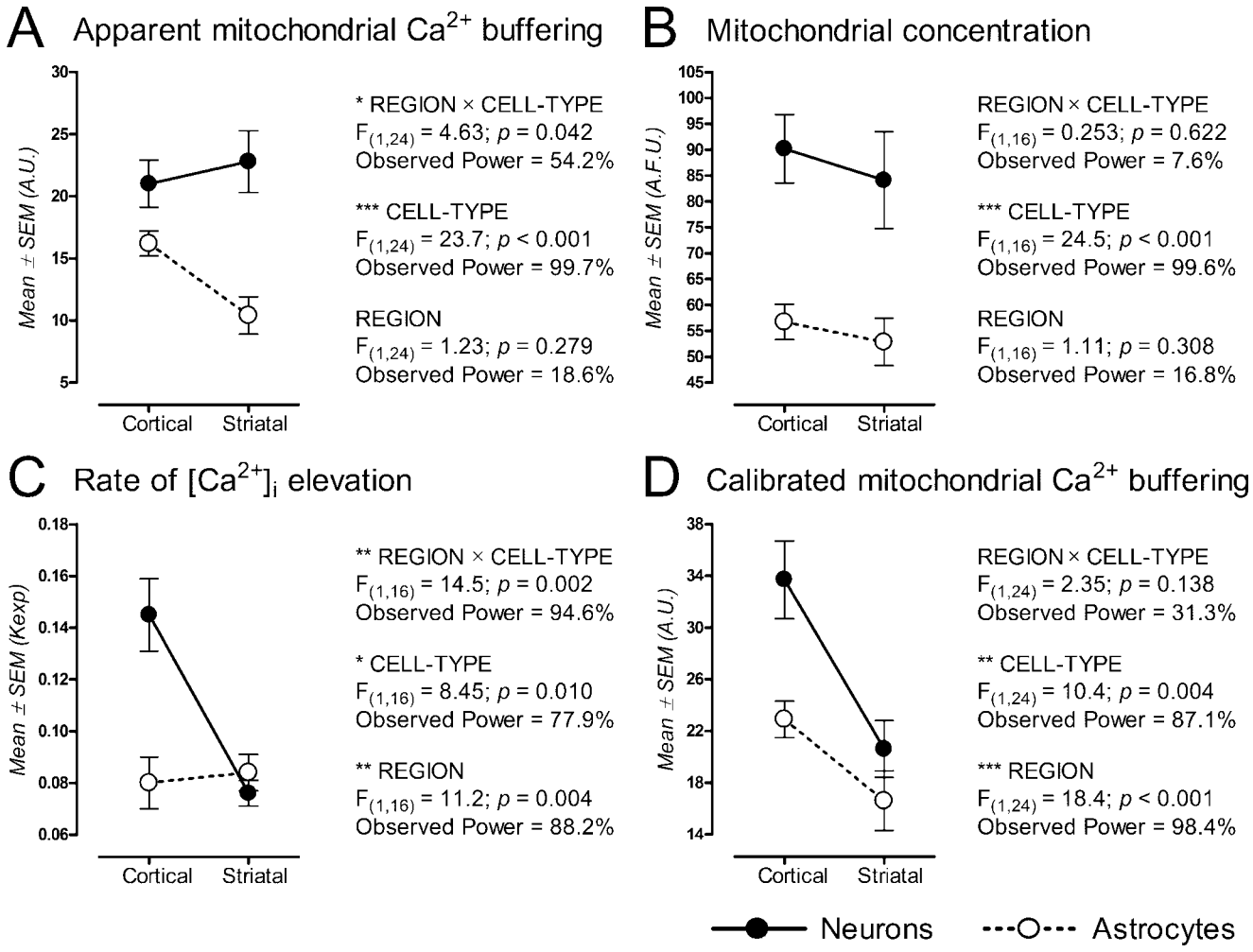

FIGURE 5. **Apparent *versus* calibrated *in situ* mitochondrial Ca^{2+} buffering capacity in cortical and striatal neurons and astrocytes.** *A–D*, factorial ANOVA profile plots, depicting mean and S.E. for the different variables (named in *graph titles*) used in analysis of variance with two factors: cell type (neurons or astrocytes; *black* or *white circles*, connected by *solid* or *dashed lines*, respectively) and region (cortical or striatal; *left* or *right circles*, respectively). Associated statistical information is shown on the *right* of each *graph* (*, $p < 0.05$; **, $p < 0.01$; ***, $p < 0.001$; observed power was computed using $\alpha = 0.05$). Shown are data from 5–7 independent experiments. *A.U.*, arbitrary units; *A.F.U.*, arbitrary fluorescence units. See "Results" for a detailed description of data and statistics.

chondria were isolated, we calibrated the "apparent values" for each cell type (Fig. 5*A*), dividing them by the respective average mitochondrial concentrations (Fig. 5*B*) and multiplying by the respective average rates of $[Ca^{2+}]_i$ elevation (Fig. 5*C*) $\times$ 10^3. Two-factor (region $\times$ cell type) ANOVA of the calibrated values (Fig. 5*D*) revealed a significant main effect of the cell type (neurons *versus* astrocytes; $F_{(1,24)} = 10.4$; $p = 0.004$) and of brain region (cortical *versus* striatal; $F_{(1,24)} = 18.4$; $p < 0.001$), with no significant region $\times$ cell type interaction ($F_{(1,24)} = 2.35$; $p = 0.138$). The observed power for the main effect of cell type and of brain region was 87.1 and 98.4%, respectively. Meaningfully, these results provide original evidence that mitochondria not only in neurons but also in astrocytes from striatal origin exhibit a decreased Ca^{2+} buffering capacity when compared with their cortical counterparts.

Mechanisms Underlying in Situ Mitochondrial Ca^{2+} Buffering Differences—Mitochondria have been shown to interact with the endoplasmic reticulum (ER) in the regulation of intracellular Ca^{2+} signaling (22). Thus, a possible mechanism underlying differences in *in situ* mitochondrial Ca^{2+} buffering between cell types might involve heterogeneity in their ER Ca^{2+} levels and/or ER-mitochondria Ca^{2+} signaling. To test this hypothesis, we challenged cortical and striatal cells with 1 μM thapsigargin prior to the determination of mitochondrial Ca^{2+} buffering capacity. Thapsigargin acutely and selectively arrests ER Ca^{2+} pumps, depleting and preventing ER Ca^{2+} storage (23, 24). We consistently observed transient $[Ca^{2+}]_i$ elevations following acute exposure to thapsigargin in astrocytes but less frequently in neurons (see supplemental Fig. 3 for representative tracings). Previous studies evidenced typically small Ca^{2+} increases in neurons challenged with thapsigargin, detected with the high affinity Fura-2 probe (25), which may escape detection with the intermediate affinity Fura-4F in our experiments. Although this suggests that ER stores may differ in neurons and astrocytes, thapsigargin treatment did not significantly ($p > 0.05$) modify the mitochondrial Ca^{2+} buffering capacity of each cell type (as a percentage of respective control: cortical neurons = 97.3 $\pm$ 5.8%, cortical astrocytes = 92.4 $\pm$ 2.3%, striatal neurons = 95.1 $\pm$ 2.2%, striatal astrocytes = 96.7 $\pm$ 5.8%; $n = 3$ independent experiments), arguing against a

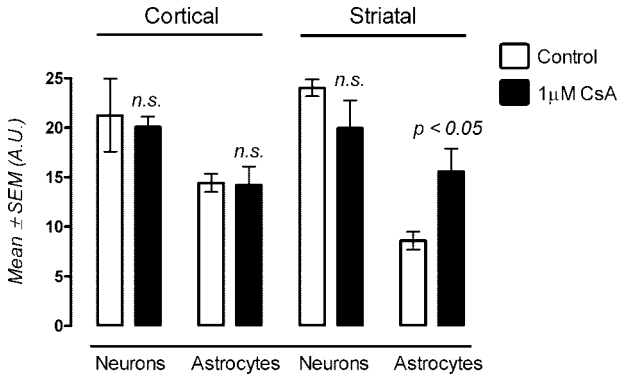

FIGURE 6. **Effect of cyclosporin A on the mitochondrial Ca^{2+} buffering capacity of intact neurons and astrocytes from cortex and striatum.** *Bars*, mean and S.E. of "apparent mitochondrial Ca^{2+} buffering capacity," assessed in experiments identical to those described in Figs. 3 and 5*A*, and performed in the absence (control; *white bars*) or presence of cyclosporin A (1 μM CsA, *black bars*). Data are from three independent experiments and were analyzed by *t* test comparison between CsA-treated cells and their respective controls, evidencing a significant ($p < 0.05$) effect in striatal astrocytes but not in other cell types (*n.s.*, nonsignificant).

major contribution of the ER in explaining differences in mitochondrial Ca^{2+} buffering between cortical and striatal neurons and astrocytes.

Differences in Ca^{2+} buffering between isolated brain mitochondria mixtures have been previously associated with the occurrence of permeability transition and/or the levels of mitochondrial cyclophilin D (26, 27). Thus, we tested whether cyclosporin A (CsA; an inhibitor of mitochondrial permeability transition that binds to cyclophilin D) influenced the differences in mitochondrial Ca^{2+} buffering exhibited by intact neurons and astrocytes. We performed experiments identical to those described in the legend to Fig. 3, both in the absence (control) and in the continuous presence of 1 μM CsA, including a 15-min preincubation period. Interestingly, results depicted in Fig. 6 showed that this CsA treatment significantly increased mitochondrial Ca^{2+} buffering capacity in striatal but not cortical astrocytes and not in neurons from either brain regions. Still, because CsA is also known to inhibit calcineurin, and thereby regulate mitochondrial phenomena such as fragmentation (28), we also tested the effect of FK506, which shares the property of calcineurin inhibition with CsA but has no effect on mitocondrial permeability transition (29). Cells were preincubated for 15 min with FK506, which was kept throughout the experiments at the previously used concentration of 0.6 μM (28). We found no significant differences ($p > 0.05$) in mitochondrial Ca^{2+} buffering between control cells and those where calcineurin was inhibited (as a percentage of respective control: cortical neurons = 96.4 ± 3.2%, cortical astrocytes = 95.8 ± 2.4%, striatal neurons = 103.9 ± 3.5%, striatal astrocytes = 93.6 ± 4.2%; $n = 3$ independent experiments). Taken together, these findings suggest that the selective effect of CsA on striatal astrocytes is unrelated to calcineurin inhibition but rather reflects inhibition of permeability transition. Thus, an increased propensity to undergo CsA-sensitive permeability transition in striatal astrocytes is a likely mechanistic explanation for their decreased mitochondrial Ca^{2+} buffering capacity when compared with cortical astrocytes.

DISCUSSION

The present study is the first to examine whether mitochondria in neurons and astrocytes from cortex and striatum differ in Ca^{2+} buffering capacity. Here we describe a novel strategy allowing *in situ* measurements of mitochondrial Ca^{2+} buffering in intact cells. In addition, we present evidence that mitochondria in striatal neurons and astrocytes exhibit a decreased Ca^{2+} buffering capacity when compared with their cortical counterparts. Also, we show that differences between neuronal and astrocytic mitochondria are region-specific and that mitochondrial Ca^{2+} buffering differences between cortical and striatal astrocytes are abolished with 1 μM CsA. These results provide additional insight into the mechanisms of selective striatal neurodegeneration and into the relative Ca^{2+} vulnerability of neuronal and astrocytic mitochondria, as discussed below.

Mitochondria are high capacity Ca^{2+} buffering systems that play a key role in protecting cells from Ca^{2+}-induced damage (17, 30). Hence, differences in mitochondrial Ca^{2+} buffering are hypothesized to assist the selective vulnerability of cellular populations in the brain. A previous study, using mitochondria isolated from cortical and striatal homogenates, raised the hypothesis that striatal mitochondria might be "supersensitive to Ca^{2+}," thus contributing for selective striatal vulnerability in HD (2). However, data reflected a mixed nonsynaptic mitochondrial population in which the predominance of neuronal (26) or glial (31) mitochondria is debatable. The ensuing question of whether striatal mitochondrial vulnerability involves neuronal or glial mitochondria or both has so far remained unanswered.

Results in this study support the last possibility by showing that mitochondrial Ca^{2+} buffering capacity is decreased not only in striatal *versus* cortical neurons but also in striatal *versus* cortical astrocytes. This implies that striatal neurons, in addition to the vulnerability present in their own mitochondria, are paired with more vulnerable astrocytic partners than cortical neurons. Also, our finding that 1 μM CsA selectively increased mitochondrial Ca^{2+} buffering capacity in striatal astrocytes, rendering it identical to that of cortical astrocytes, without modifying neuronal mitochondrial Ca^{2+} buffering, has important implications. Indeed, it suggests that the ability of CsA to protect striatal neurons in *in vivo* HD models (32) could be the indirect consequence of reducing the mitochondrial vulnerability of their astrocytic neighbors.

Vulnerable astrocytes may aggravate the susceptibility of neuronal neighbors by failing to provide adequate support under pathophysiological conditions (9, 11, 33). Mitochondrial impairment in astrocytes may compromise protective astrocyte-neuron lactate trafficking and/or cause them to produce diffusible reactive oxygen species that damage nearby neurons (10, 34). Meaningfully, neurons rely on astrocytes for an efficient clearance of extracellular glutamate, an activity shown to be defective in HD astrocytes (35). We propose that deficits in this and other energy-dependent astrocytic activities will be aggravated in striatal astrocytes, since their Ca^{2+}-vulnerable mitochondria should more frequently arrest ATP synthase or even reverse its activity, thus decreasing ATP availability.

ATP synthase reversal allows mitochondria to delay $\Delta\psi_m$ collapse, provided that cells have sufficient glycolytic ATP. Thus, mitochondria may appear to be more resistant to injury in cells with abundant glycogen stores, as we have previously shown for HD cellular models (8). Given the limited glycogen availability in neurons as opposed to astrocytes (36), the phenomenon of $\Delta\psi_m$ maintenance by ATP synthase reversal may better conceal earlier mitochondrial damage in astrocytes than in neurons, thus acting as a major confounding factor when comparing mitochondrial function in these cell types. To avoid this, we inhibited the use of glycogen stores and ATP synthase reversal in our experiments with intact neurons and astrocytes. For the purpose of data comparison, it should be noted that glycogen stores are typically unavailable in isolated mitochondria experiments.

Isolated brain mitochondria are mixtures of neuronal and glial mitochondria. These mixtures are heterogeneous in response to Ca^{2+}, as shown within nonsynaptic fractions (37), and when comparing synaptic with nonsynaptic fractions (26, 27), strengthening the hypothesis that neurons and glia differ in Ca^{2+} buffering capacity. Presently, it is still unfeasible to isolate functional neuronal and glial mitochondria from the adult brain, narrowing the pursuit of this hypothesis to studies with primary cultures of brain cells. A previous study addressed this hypothesis using suspensions of permeabilized cells and evidenced that mitochondria in cerebellar neurons (1 DIV) buffered less Ca^{2+} than in cortical astrocytes (10 DIV) (38). However, given the different regions under study for neurons (cerebellum) and astrocytes (cortex), it cannot be generalized that neuronal mitochondria buffer less Ca^{2+} than astrocytic mitochondria. Indeed, within the same region (cortex or striatum), we saw the opposite, namely that neuronal mitochondria buffered more Ca^{2+} than astrocytic mitochondria. Still, this did not apply across regions, since mitochondria in striatal neurons did not buffer more Ca^{2+} than in cortical astrocytes, highlighting the cellular and regional specificity of mitochondrial Ca^{2+} buffering differences.

Addressing the mechanisms underlying mitochondrial Ca^{2+} buffering differences and considering possible mitochondria-ER interactions in Ca^{2+} signaling (22), we tested whether selectively depleting and arresting ER Ca^{2+} pumps with thapsigargin modified *in situ* mitochondrial Ca^{2+} buffering. Because thapsigargin did not significantly affect mitochondrial Ca^{2+} buffering in any of the four cell types, it is unlikely that ER heterogeneity explains their differences in mitochondrial Ca^{2+} buffering capacity. This finding by no means undermines the physiological relevance of ER-mitochondria Ca^{2+} signaling, particularly at low $[Ca^{2+}]_i$, being probably explained by the wide disparity in the amounts of maximal Ca^{2+} accumulation by the two organelles and by ER saturation occurring before $[Ca^{2+}]_i$ reaches the set point for mitochondria net uptake. Although intact cells may differ in Ca^{2+} handling mechanisms other than the mitochondria (*e.g.* pumps, buffers, and exchangers), in our experimental conditions, we have introduced calibrations for the rate of Ca^{2+} elevation (K_{exp}) in the different cell types when mitochondria Ca^{2+} buffering was selectively inhibited, which yielded a measurement of net $[Ca^{2+}]_i$ elevation considering Ca^{2+} handling mechanisms (entry and extrusion pathways) other than the mitochondria.

Alternative mechanisms may involve a differential mitochondrial sensitivity to permeability transition. We tested whether mitochondrial Ca^{2+} buffering was modified by CsA (inhibitor of permeability transition and calcineurin), and by FK506 (calcineurin inhibitor). The absence of effect of FK506 suggests that calcineurin activity does not modify mitochondrial Ca^{2+} buffering, possibly because calcineurin activation is subsequent to mitochondrial depolarization (28), when the driving force for Ca^{2+} buffering is exhausted. Moreover, it highlights the inhibition of permeability transition rather than calcineurin as the prevailing effect of CsA in our experiments. Therefore, given that 1 μM CsA abolished the differences in *in situ* mitochondrial Ca^{2+} buffering between cortical and striatal astrocytes, our results show that mitochondria in striatal astrocytes exhibit an increased propensity to undergo a CsA-sensitive form of permeability transition. The lack of a CsA (1 μM) effect over the other cell types suggests the occurrence of CsA-insensitive forms of permeability transition (39, 40). However, it is also possible that higher concentrations of CsA might be required for an effect to be observable, as suggested from recent data with isolated synaptic mitochondria, where 5 μM but not 1 μM CsA increased mitochondrial Ca^{2+} buffering capacity (27). Unfortunately, testing of this possibility in intact neurons is hampered by their vulnerability to greater than 1 μM CsA concentrations (39, 41). The need for high CsA concentrations in order to inhibit mitochondrial permeability transition may be associated with high levels of the CsA target, cyclophilin D (CypD) (27). Indeed, CypD levels were shown to be inversely correlated with the mitochondrial resistance to permeability transition, namely throughout brain development (42). Meaningfully, the highest levels of brain CypD protein were found in 1-day-old rats and progressively decreased, so that at 10 days of age, CypD expression became nearly identical to that of mature 3-month-old animals (Fig. 4*d* in Ref. 42). These findings suggest that the relative differences in mitochondrial Ca^{2+} vulnerability between 1 DIV cerebellar neurons and 10 DIV cortical astrocytes (38) might change considerably when both cell types have 10 DIV. Moreover, the stabilization of CypD expression after 10 days of age (42) supports the modeling of brain mitochondrial Ca^{2+} buffering with mature cultures of brain cells (11–13 DIV in the present study). Indeed, sufficient time in culture is essential for neurons to develop a network of processes containing mitochondria that is probably heterogeneous with respect to that in the cell body (43–45).

The decreased mitochondrial Ca^{2+} buffering of striatal *versus* cortical neurons in the present study reflects neuronal mitochondria as a whole. In light of recent findings with synaptic *versus* nonsynaptic cortical mitochondria (26), it would be interesting to compare the Ca^{2+} vulnerability of synaptic mitochondria in striatal and cortical neurons, since it may contribute to differences in the present study and influence pathological synaptic dysfunction in HD (46) as well as the greater susceptibility of striatal neurons to toxic insults (1, 6, 47). We recently compared the distribution and trafficking of *in situ* mitochondria within the processes of cortical and striatal neurons and found similar fractional occupations but faster mito-

chondria movement in cortical neurons.[3] Although similar mitochondrial fractional occupation in processes is in agreement with the similar overall mitochondrial concentrations reported in the present study, the differences in mitochondrial movement speed raise the interesting hypothesis that mitochondria in cortical neurons may more rapidly and efficiently handle Ca^{2+} buffering needs in distant processes by means of faster trafficking.

In summary, the present study shows for the first time that the increased vulnerability of striatal *versus* cortical mitochondria to Ca^{2+} loads resides in both intact neurons and astrocytes. Mitochondria in striatal astrocytes have an increased propensity to undergo CsA-sensitive permeability transition, positioning the striatum at greater risk for disturbed neuron-astrocyte interactions and probably contributing to selective striatal demise in HD and other neurological disorders. The selective effect of 1 μM CsA over striatal astrocytes suggests that *in vivo* neuronal sheltering with this compound may indirectly result from astrocytic protection.

REFERENCES

1. Calabresi, P., Centonze, D., and Bernardi, G. (2000) *Neurology* **55,** 1249–1255
2. Brustovetsky, N., Brustovetsky, T., Purl, K. J., Capano, M., Crompton, M., and Dubinsky, J. M. (2003) *J. Neurosci.* **23,** 4858–4867
3. Li, S. H., Schilling, G., Young, W. S., III, Li, X. J., Margolis, R. L., Stine, O. C., Wagster, M. V., Abbott, M. H., Franz, M. L., Ranen, N. G., Folstein, S. E., Hedreen, J., and Ross, C. A. (1993) *Neuron* **11,** 985–993
4. Rosas, H. D., Salat, D. H., Lee, S. Y., Zaleta, A. K., Pappu, V., Fischl, B., Greve, D., Hevelone, N., and Hersch, S. M. (2008) *Brain* **131,** 1057–1068
5. Vonsattel, J. P., and DiFiglia, M. (1998) *J. Neuropathol. Exp. Neurol.* **57,** 369–384
6. Cowan, C. M., and Raymond, L. A. (2006) *Curr. Top. Dev. Biol.* **75,** 25–71
7. Nicholls, D. G., and Budd, S. L. (2000) *Physiol. Rev.* **80,** 315–360
8. Oliveira, J. M., Chen, S., Almeida, S., Riley, R., Goncalves, J., Oliveira, C. R., Hayden, M. R., Nicholls, D. G., Ellerby, L. M., and Rego, A. C. (2006) *J. Neurosci.* **26,** 11174–11186
9. Lobsiger, C. S., and Cleveland, D. W. (2007) *Nat. Neurosci.* **10,** 1355–1360
10. Bambrick, L., Kristian, T., and Fiskum, G. (2004) *Neurochem. Res.* **29,** 601–608
11. Dienel, G. A., and Hertz, L. (2005) *Glia* **50,** 362–388
12. Nicholls, D. G. (2006) *J. Biol. Chem.* **281,** 14864–14874
13. Oliveira, J. M., Jekabsons, M. B., Chen, S., Lin, A., Rego, A. C., Goncalves, J., Ellerby, L. M., and Nicholls, D. G. (2007) *J. Neurochem.* **101,** 241–249
14. Ward, M. W., Rego, A. C., Frenguelli, B. G., and Nicholls, D. G. (2000) *J. Neurosci.* **20,** 7208–7219
15. Haugland, R. P. (2002) *Handbook of Fluorescent Probes and Research Products*, pp. 776–781, Molecular Probes, Inc., Eugene, OR
16. Wokosin, D. L., Loughrey, C. M., and Smith, G. L. (2004) *Biophys. J.* **86,** 1726–1738
17. Nicholls, D. G. (2005) *Cell Calcium* **38,** 311–317
18. Makowska, A., Zablocki, K., and Duszynski, J. (2000) *Eur. J. Biochem.* **267,** 877–884
19. Cho, J. H., Balasubramanyam, M., Chernaya, G., Gardner, J. P., Aviv, A., Reeves, J. P., Dargis, P. G., and Christian, E. P. (1997) *Biochem. J.* **324,** 971–980
20. Li, L., Fan, M., Icton, C. D., Chen, N., Leavitt, B. R., Hayden, M. R., Murphy, T. H., and Raymond, L. A. (2003) *Neurobiol. Aging* **24,** 1113–1121
21. Chalmers, S., and Nicholls, D. G. (2003) *J. Biol. Chem.* **278,** 19062–19070
22. Rizzuto, R., Duchen, M. R., and Pozzan, T. (2004) *Sci. STKE 2004*, re1
23. Thastrup, O., Cullen, P. J., Drobak, B. K., Hanley, M. R., and Dawson, A. P. (1990) *Proc. Natl. Acad. Sci. U. S. A.* **87,** 2466–2470
24. Lytton, J., Westlin, M., and Hanley, M. R. (1991) *J. Biol. Chem.* **266,** 17067–17071
25. Weber, J. T., Rzigalinski, B. A., and Ellis, E. F. (2001) *J. Biol. Chem.* **276,** 1800–1807
26. Brown, M. R., Sullivan, P. G., and Geddes, J. W. (2006) *J. Biol. Chem.* **281,** 11658–11668
27. Naga, K. K., Sullivan, P. G., and Geddes, J. W. (2007) *J. Neurosci.* **27,** 7469–7475
28. Cereghetti, G. M., Stangherlin, A., Martins de Brito, O., Chang, C. R., Blackstone, C., Bernardi, P., and Scorrano, L. (2008) *Proc. Natl. Acad. Sci. U. S. A.* **105,** 15803–15808
29. Friberg, H., Ferrand-Drake, M., Bengtsson, F., Halestrap, A. P., and Wieloch, T. (1998) *J. Neurosci.* **18,** 5151–5159
30. Krieger, C., and Duchen, M. R. (2002) *Eur. J. Pharmacol.* **447,** 177–188
31. Kristian, T., Hopkins, I. B., McKenna, M. C., and Fiskum, G. (2006) *J. Neurosci. Methods* **152,** 136–143
32. Leventhal, L., Sortwell, C. E., Hanbury, R., Collier, T. J., Kordower, J. H., and Palfi, S. (2000) *J. Comp. Neurol.* **425,** 471–478
33. Araque, A., Parpura, V., Sanzgiri, R. P., and Haydon, P. G. (1999) *Trends Neurosci.* **22,** 208–215
34. Rossi, D. J., Brady, J. D., and Mohr, C. (2007) *Nat. Neurosci.* **10,** 1377–1386
35. Shin, J. Y., Fang, Z. H., Yu, Z. X., Wang, C. E., Li, S. H., and Li, X. J. (2005) *J. Cell Biol.* **171,** 1001–1012
36. Brown, A. M. (2004) *J. Neurochem.* **89,** 537–552
37. Kristian, T., Weatherby, T. M., Bates, T. E., and Fiskum, G. (2002) *J. Neurochem.* **83,** 1297–1308
38. Bambrick, L. L., Chandrasekaran, K., Mehrabian, Z., Wright, C., Krueger, B. K., and Fiskum, G. (2006) *J. Bioenerg. Biomembr.* **38,** 43–47
39. Brustovetsky, N., and Dubinsky, J. M. (2000) *J. Neurosci.* **20,** 8229–8237
40. Chinopoulos, C., Starkov, A. A., and Fiskum, G. (2003) *J. Biol. Chem.* **278,** 27382–27389
41. McDonald, J. W., Goldberg, M. P., Gwag, B. J., Chi, S. I., and Choi, D. W. (1996) *Ann. Neurol.* **40,** 750–758
42. Eliseev, R. A., Filippov, G., Velos, J., VanWinkle, B., Goldman, A., Rosier, R. N., and Gunter, T. E. (2007) *Neurobiol. Aging* **28,** 1532–1542
43. Sonnewald, U., Hertz, L., and Schousboe, A. (1998) *J. Cereb. Blood Flow Metab.* **18,** 231–237
44. Collins, T. J., Berridge, M. J., Lipp, P., and Bootman, M. D. (2002) *EMBO J.* **21,** 1616–1627
45. Kann, O., and Kovacs, R. (2007) *Am. J. Physiol. Cell Physiol.* **292,** C641–657
46. Smith, R., Brundin, P., and Li, J. Y. (2005) *Cell Mol. Life Sci.* **62,** 1901–1912
47. Garcia, J. H., Liu, K. F., and Ho, K. L. (1995) *Stroke* **26,** 636–643

[3] J. M. A. Oliveira, I. Prokopová, P. Guedes-Dias, and J. Gonçalves, unpublished observation.